PHYSICAL REVIEW B VOLUME 4, NUMBER 3 1 AUGUST 1971

Neutron-Scattering Study of TmSb: A Model Crystal-Field-Only Metallic Paramagnet

R. J. Birgeneau* and E. Bucher
Bell Laboratories, Murray Hill, New Jersey 07974
and
L. Passell
Brookhaven National Laboratory,† Upton, New York 11973
and
K. C. Turberfield
Atomic Energy Research Establishment, Harwell, England
(Received 6 April 1971)

Inelastic-neutron-scattering studies have been carried out on the paramagnetic metallic compound TmSb. The Tm^{3+} ground-state multiplet $^3H_6$ is split by the octahedral crystal field into six levels Γ_1, Γ_4, $\Gamma_5^{(2)}$, Γ_2, $\Gamma_5^{(1)}$, Γ_3. Transitions between these levels have been observed and the parameters $A_4\langle r^4\rangle = (6.86 \pm 0.10)$ meV, $A_6\langle r^6\rangle = (0.44 \pm 0.04)$ meV have been deduced. The fourth-order term is consistent with that expected on the basis of a simple nearest-neighbor point-charge model, whereas the sixth-order term is an order of magnitude too large; this is in marked contrast with previous results in PrSb and other praseodymium pnictides and chalcogenides where the effective-point-charge model is quantitatively correct for both terms. It is found that the actual spectra can be reproduced in detail using ordinary crystal-field theory together with a simple approximation to the instrumental-resolution function. Furthermore, no appreciable exchange broadening of the transitions is observed at low temperatures, thus confirming TmSb as a model crystal-field-only metallic paramagnet.

I. INTRODUCTION

The rare-earth monopnictides and monochalcogenides provide a set of compounds which exhibit a plethora of interesting and occasionally bizarre physical properties.[1,2] These vary from ferromagnetic semiconduction in EuO,[3] to a pressure-induced insulator-metal transition in SmS,[4] to magnetic ordering in the singlet ground-state system TbSb due to a polarization instability,[5] to spontaneous nuclear ordering at 10 m°K in PrBi.[6] The magnetic properties of many of the compounds are particularly interesting because of the fact that crystal-field and exchange energies are often of the same order of magnitude. In order to understand the magnetic properties it is first necessary to have some detailed knowledge of the nature and magnitude of the crystal field. In turn, it seems likely that a systematic study of Stark splittings in these compounds could lead to a proper understanding of the microscopic origins of crystal fields in metals. The rare-earth monopnictides and monochalcogenides are particularly well suited for such a study since they have the combined advantages of the simple rock-salt structure together with wide variations in lattice constants, $4f$ radius, and carrier concentration.

Recently, we have shown[7–9] that in rare-earth metallic compounds in which the exchange field is somewhat weaker than the crystal field, inelastic-neutron-scattering techniques can provide detailed knowledge of the single-ion crystal-field-level energies and wave functions. A systematic study of the compounds PrBi, PrSb, PrAs, PrP, PrTe, PrSe, and PrS was carried out, and it was found that in general the observed neutron spectra could be reproduced in detail theoretically using ordinary crystal-field theory. Furthermore, the actual crystal-field parameters so obtained could be quantitatively accounted for using a simple nearest-neighbor point-charge model with a ligand charge of -2. This latter result was most unexpected and indeed it remains unexplained.

It is clearly of interest to extend these measurements to other systems. In this paper we report a detailed study of crystal-field effects in TmSb using inelastic-neutron-scattering techniques. TmSb was chosen for study for several reasons. First, the configuration of Tm^{3+} is $4f^{12}$, so that it is complementary to that of Pr^{3+}, $4f^2$. However, the $4f$ radius in Tm^{3+} is considerably smaller than that in Pr^{3+},[10] so that this should provide a stringent test of the effective-point-charge model. Second, extensive single-crystal high-field magnetization measurements on TmSb and $Tm_{0.53}Y_{0.47}$Sb have been reported by Cooper and Vogt.[11] They find that the magnetization can be accurately predicted using simple crystal-field theory with no exchange whatsoever. They then suggest that TmSb can be regarded as a model rare-earth inter-

metallic compound exhibiting crystal-field effects alone. Therefore, it is of some interest to perform direct spectroscopic measurements on TmSb to test this conjecture. Finally, TmSb supplies a somewhat greater challenge experimentally than the praseodymium compounds that have already been studied. First, the Tm^{3+} energy-level diagram is somewhat more complex than that for Pr^{3+} with nine, as opposed to four, allowed transitions. Second, some of the transition probabilities depend on the crystal-field parameters themselves, since one representation (Γ_5) occurs twice. Third, the crystal-field energies are such that transitions can be seen in both neutron energy loss and energy gain; this gives a stricter test of the theory of the instrument employed in the numerical convolutions.

The format of the paper is as follows. Section II gives a brief outline of the crystal-field and neutron-scattering theory for the Tm^{3+} ion. In Sec. III we describe the experimental methods and the experimental results. In Sec. IV, a detailed analysis of the spectra using the crystal-field model is given. Finally, in Sec. V the results are discussed in the context of both the point-charge model and the Pr^{3+} compound parameters and general conclusions are drawn.

II. THEORY

The Tm^{3+} ion has the configuration $4f^{12}$ with the $^3H_6$ multiplet lying lowest. The next-highest multiplet $^3H_4$ lies at ~ 5500 cm^{-1}, [12] and may be ignored in the discussion of the much smaller splitting of the ground-state multiplet. For a cubic system the crystal-field Hamiltonian may be written[13]

$$\mathcal{H}_{CF} = A_4\langle r^4\rangle \chi_4 (O_4^0(J) + 5O_4^4(J)) + A_6\langle r^6\rangle \chi_6 (O_6^0(J) - 21O_6^4(J)) \quad , \quad (1)$$

where the O_n^m are Stevens operator equivalents and the χ_n are reduced matrix elements. [14] $A_4\langle r^4\rangle$ and $A_6\langle r^6\rangle$ are the numerical coefficients in the tesseral harmonic expansion of the electrostatic potential at the Tm^{3+} site. For the rock-salt structure the nearest-neighbor point-charge contribution to the potential is given by

$$A_4\langle r^4\rangle = \tfrac{7}{16}(Ze^2/R^5)\langle r^4\rangle \quad , \qquad A_6\langle r^6\rangle = \tfrac{3}{64}(Ze^2/R^7)\langle r^6\rangle \quad , \quad (2)$$

where Ze is the effective charge at the ligand site.

Following Lea, Leask, and Wolf[15] (hereafter denoted LLW), it is convenient to introduce new parameters W, x defined by

$$A_4\langle r^4\rangle \chi_4 F(4) = Wx \quad , \qquad A_6\langle r^6\rangle \chi_6 F(6) = W(1 - |x|) \quad , \quad (3)$$

where $-1 < x < 1$ and $F(4)$, $F(6)$ are numerical factors tabulated by LLW. Equation (1) then becomes

$$\mathcal{H}_{CF} = W\left(x\frac{1}{F(4)}(O_4^0 + 5O_4^4) + (1 - |x|)\frac{1}{F(6)}(O_6^0 - 21O_6^4)\right), \quad (4)$$

so that W functions as a simple scale factor and x measures the relative size of the fourth- and sixth-order terms. As x is varied between -1 and $+1$, $A_4\langle r^4\rangle \chi_4 / A_6\langle r^6\rangle \chi_6$ goes from $-\infty$ to $+\infty$. LLW have diagonalized Eq. (4) for all values of x and for all J. The results for the $J = 6$ appropriate to Tm^{3+} are shown in Fig. 1(a). From the

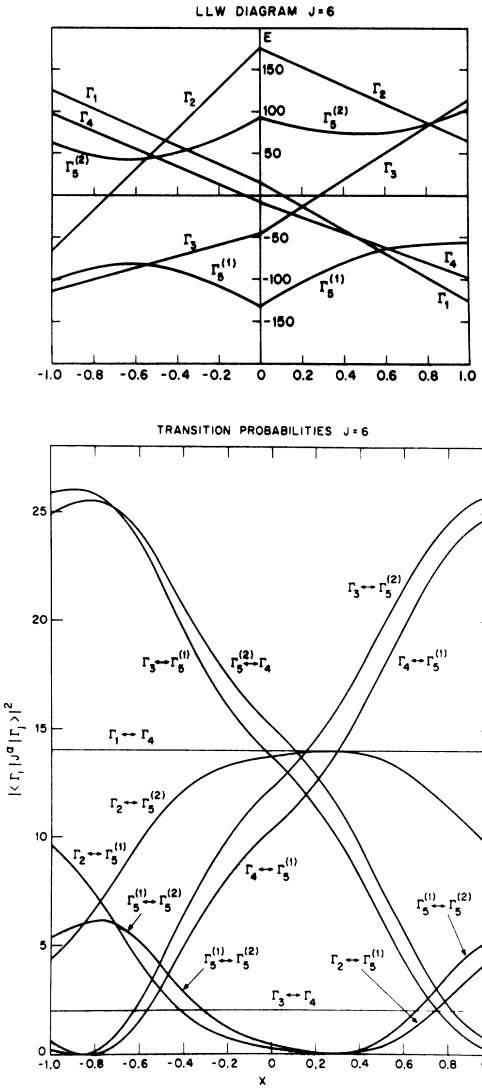

FIG. 1. (a) Eigenvalues of Eq. (4) in units of W as a function of the LLW parameter x. (b) Transition probabilities for $J = 6$ in a cubic crystal field as a function of the LLW parameter x.

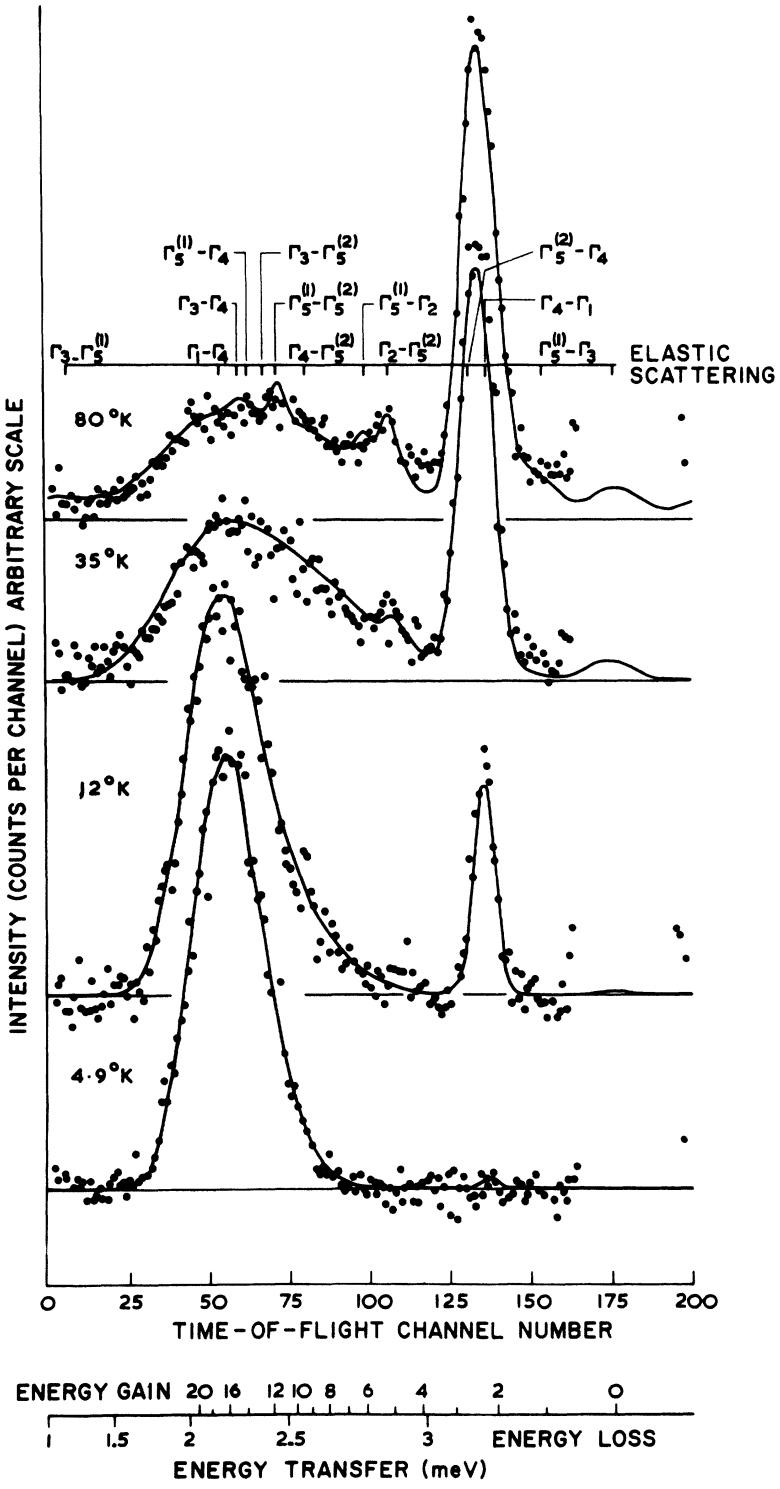

FIG. 2. Time-of-flight neutron spectra for TmSb as a function of temperature. Smooth curves and associated background levels represent the results of theoretical fits to the data as described in the text.

figure it may be seen that the $J=6$ multiplet is split into two singlets Γ_1, Γ_2, a doublet Γ_3, and three triplets Γ_4, $\Gamma_5^{(1)}$, $\Gamma_5^{(2)}$. Only the $\Gamma_5^{(i)}$ eigenfunctions depend explicitly on x.

Substitution in (2) and (3) for $\langle r^n \rangle$, χ_n, R yields point-charge estimates of

$$W = -0.0203Z \text{ meV}, \qquad x = -0.955 \tag{5}$$

for Tm^{3+} in TmSb, so that both x and W are nega-

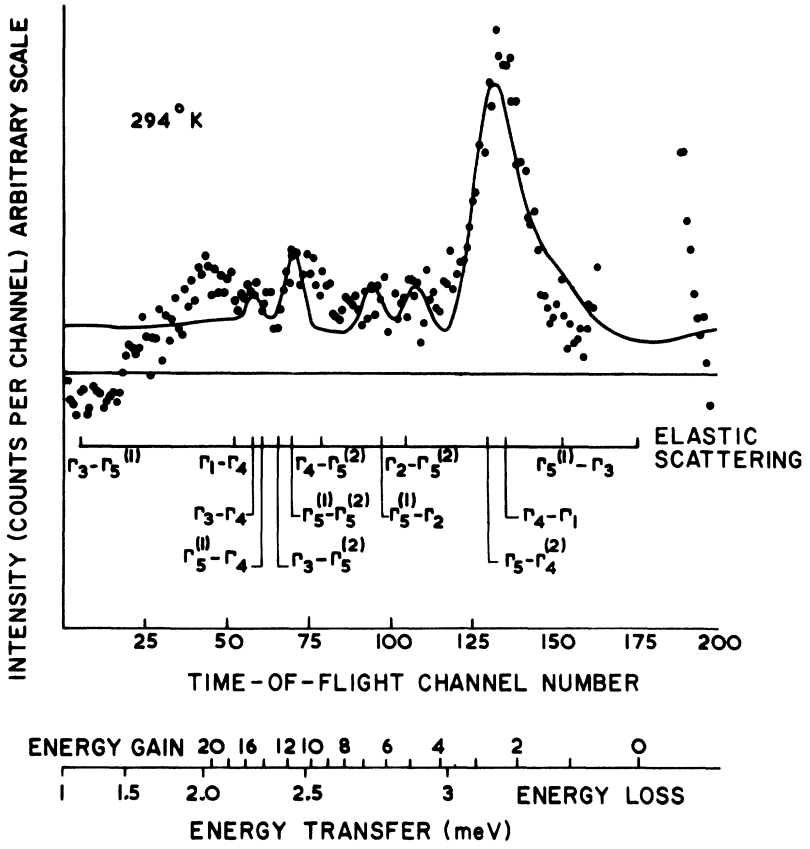

FIG. 3. Time-of-flight neutron spectra for TmSb at 294°K.

tive. From their single-crystal measurements Cooper and Vogt[11] conclude that x lies in the range $-1.0<x<-0.6$ and that W is ~ -0.08 meV; this is consistent with the values predicted by (5). Examination of Fig. 1(a) shows that these approximate values for x, W necessitate that the energy levels be in the order Γ_1, Γ_4, $\Gamma_5^{(2)}$, Γ_2, $\Gamma_5^{(1)}$, Γ_3 with typical spacings of 3 meV.

The neutron-scattering cross section at small momentum transfers in the single-ion approximation may be written[16]

$$\frac{\partial^2\sigma}{\partial\Omega_f\partial\omega_f} = e^{-2W}\left(\frac{1.91e^2}{2mc^2}g_J\right)^2\frac{k_f}{k_i}F^2(\vec{Q}) \times\sum_{n,m}\rho_n|\langle n|\vec{J}_\perp|m\rangle|^2\delta\left(\frac{E_n-E_m}{\hbar}-\omega\right), \tag{6}$$

where $\vec{J}_\perp$ is the component of the total angular momentum perpendicular to the scattering vector $\vec{Q}$. The other symbols have their usual meaning. We have discussed Eq. (6) at length in Ref. 9. Here it is sufficient to point out that Eq. (6) implies that at small momentum transfers the scattering should obey magnetic dipole selection rules. Birgeneau[17] has tabulated the $|\langle\Gamma^i|\vec{J}_\perp|\Gamma^j\rangle|^2$ for all values of x and for all J. The results for $J=6$ are shown in Fig. 1(b). There are nine allowed transitions in all with the relative intensities shown in the figure; for the range of x values expected from Cooper and Vogt's results, at least six of these nine allowed transitions should be intense enough to be observable, provided, of course, that the levels from which the transitions originate have an appreciable thermal population. For the energy-level diagram proposed above, two of the three most intense transitions, $\Gamma_1 \rightarrow \Gamma_4$ and $\Gamma_5^{(2)} \rightarrow \Gamma_4$, should in fact be observable at relatively low temperatures.

III. EXPERIMENTAL METHODS AND RESULTS

The experiments were carried out on the "slow chopper" neutron time-of-flight spectrometer at the Brookhaven high flux beam reactor. The characteristics of this instrument and the details of the experimental method have been discussed at length in Ref. 9. The incident neutrons had a wavelength of 4.1 Å corresponding to an energy of 4.9 meV. The sample[18] which was in the form of a powder was placed in an aluminum container 2 mm thick by 1 cm by 3 cm. The small thickness was necessary because of the large absorption cross section of thulium (71×10^{-24} cm^2 at 1.08 Å).

The sample was mounted in a Cryogenics Associates temperature-controlled Dewar which could be varied continuously between 4.2 °K and room temperature. Typical counting times were 24 h at each temperature. Data were collected in sets of 6, 5, and 3 counters spaced about 1° apart with their centroids at 27°, 42°, and 99°, respectively, from the forward direction. For typical energy transfers these give momentum transfers varying from $|\vec{Q}|/4\pi \sim 0.12$ to 0.25 Å^{-1} so that the dipole approximation, Eq. (6), for the neutron-scattering cross section should be quite satisfactory. In addition, the $\vec{Q}$ dependence of the peak intensities is automatically determined. This latter feature is important because it enables one to distinguish between lattice vibrations and magnetic excitations, the former varying as $|\vec{Q}|^2$ and the latter as $F^2(\vec{Q})$.

Typical experimental spectra obtained at 4.9, 12, 35, 80, and 294°K are shown in Figs. 2 and 3. From the figures it may be seen that the spectra exhibit a rich amount of detail which changes markedly with temperature. In order to explain the basic features of the scattering, it is first necessary to describe more explicitly the characteristics of the time-of-flight spectrometer in the context of Fig. 2. The peak centered about channel 176 corresponds to neutrons elastically scattered from the sample. Neutrons arriving in channels preceding No. 176 have a velocity and hence energy greater than that of the elastically scattered neutrons, so that they have gained energy from the system. This corresponds to an *energy-gain* process in which the Tm^{3+} ion is deexcited from a higher to a lower level. On the other hand, neutrons to the right of channel 176 have a velocity and hence energy less than that of the incident neutrons, so that they have lost energy to the system; this is called an *energy-loss* process.

This would present no conceptual problem except for the fact that there are only 204 8-μsec time channels available in all (the number of channels being determined by the time interval between successive bursts of incident neutrons). The spectra from successive neutron bursts are then superimposed on each other with a time separation of 204 channels or $8 \times 204 = 1632$ μsec between elastic peaks. Thus, for example, a neutron with a velocity such that it would arrive at the detector at a time corresponding to channel 250 instead appears in $250 - 204 = 46$ in the spectrum. Accordingly, in Figs. 2 and 3 we have given energy scales which correspond to both energy gain and energy loss. As we shall see, the two processes are easily distinguished from each other.

IV. ANALYSIS

As noted in Sec. II, both Cooper and Vogt's results and the point-charge model indicate that the energy levels are in the order Γ_1, Γ_4, $\Gamma_5^{(2)}$, Γ_2, $\Gamma_5^{(1)}$, Γ_3. The consequent energy-level diagram together with the corresponding allowed transitions are given in Fig. 4. The magnetization measurements of Cooper and Vogt and also Schottky anomaly measurements by Bucher *et al.*[19] give the $\Gamma_1 \rightarrow \Gamma_4$ separation as 2.3 ± 0.1 meV. From Fig. 4 it may be seen that at 4.9 °K we would only expect to see one transition, $\Gamma_4 \rightarrow \Gamma_1$, in energy loss. The actual spectrum we observe at 4.9 °K is in excellent agreement with this prediction, that is, we see a single peak centered at -2.22 ± 0.02 meV. By 12 °K the Γ_4 level is sufficiently well populated that the $\Gamma_4 \rightarrow \Gamma_1$ transition can be seen in energy gain as well. The interpretation of the 35 °K spectrum is also straightforward. There are two significant changes in the spectrum between 12 and 35 °K. First, the peaks formerly at ± 2.22 meV have shifted to about ± 2.46 meV and have broadened considerably. Second, an additional peak has appeared at 4.8 meV. The change in the scattering at 2.22 meV is most likely due to the appearance of additional unresolved scattering originating from the $\Gamma_5^{(2)}$ level, that is, the $\Gamma_5^{(2)} \rightarrow \Gamma_4$ transition. The peak at 4.8 meV may then be identified as the $\Gamma_2 \rightarrow \Gamma_5^{(2)}$ transition. Consideration of the relative intensities predicted from Fig. 1(b) shows that these identifications are at least reasonable. These three

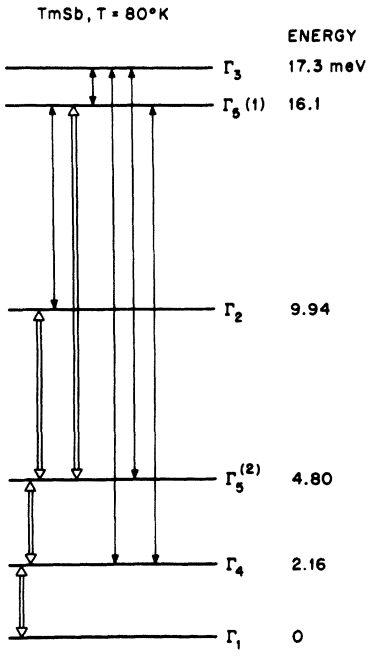

FIG. 4. Energy-level diagram for TmSb at 80 °K. The energies are those deduced from the fit to the spectrum shown in Fig. 2. Arrows indicate the allowed transitions; those with double bars are seen clearly at 80 °K.

identifications are, in fact, sufficient to determine the parameters $A_4\langle r^4\rangle$, $A_6\langle r^6\rangle$ in Eq. (1) or, equivalently, W and x in Eq. (4).

As discussed extensively in Ref. 9, once $A_4\langle r^4\rangle$ and $A_6\langle r^6\rangle$ have been determined, then the complete time-of-flight spectrum at all temperatures can be calculated using the eigenvalues and eigenfunctions determined from the diagonalization of Eq. (1). This supplies a rigorous test of the parameters $A_4\langle r^4\rangle$, $A_6\langle r^6\rangle$ and indeed of the crystal-field model itself. Accordingly, we have generalized the least-squares fitting program described in Ref. 9 so that it can be used for all J. Theoretical fits to the spectra are shown as the solid lines in Figs. 2 and 3. The adjustable parameters in the fits include $A_4\langle r^4\rangle$, $A_6\langle r^6\rangle$, one common width $\Delta\Gamma$, one over-all scaling factor, and one parameter for the background (which is assumed flat). All of the instrumental parameters have been determined separately.

We consider first the fits up to 80 °K shown in Fig. 2. Initial values for $A_4\langle r^4\rangle$, $A_6\langle r^6\rangle$ were chosen to give approximate agreement with the peak identifications discussed above. From the figure it may be seen that the fits are quite good at all temperatures. The parameters determined at 80 °K are

$$A_4\langle r^4\rangle = 6.81 \pm 0.10 \text{ meV} \ , \qquad A_6\langle r^6\rangle = 0.44 \pm 0.04 \text{ meV} \ , \tag{7}$$

or equivalently

$$W = -0.0856 \pm 0.002 \text{ meV} \ , \qquad x = -0.785 \pm 0.02 \ . \tag{8}$$

The error bars correspond to two-standard-deviation statistical errors. It should be emphasized that no reasonable fit could be obtained for values outside of these limits. The corresponding crystal-field-level energies are those given in Fig. 4. The intrinsic widths $\Delta\Gamma(T)$ are found to vary continuously from 0.08 ± 0.06 meV at 4.9 °K to 0.36 meV at 80 °K. It is assumed that these temperature-dependent widths originate in phonon and conduction-electron relaxation processes. However, we shall not consider this aspect of the problem explicitly here. The variation in the instrumental widths of the transitions evident in Fig. 2 originates in the non-linear relationship between an uncertainty in energy and the corresponding uncertainty in time of flight. The fit at 80 °K is particularly impressive; the theory is able to reproduce both the positions and the relative intensities of all the peaks. Similar agreement at 80 °K was also found in PrSb,[9] but in that case the energy-level diagram was less complex and, in addition, the transition probabilities did not depend explicitly on the crystal-field parameters. The small width observed at 4.9 °K, together with the fact that the energy-gain and energy-loss peak energies at 12 °K match exactly in all counters, indicates that the dispersion in the crystal-field excitons is negligible.

From Fig. 3 we see that at room temperature the crystal-field model is no longer able to account for all of the scattering. In particular, there is intense scattering centered about 25 meV which is not predicted for the magnetic system, although all of the peaks at lower energies seem to be properly accounted for. This residual peak undoubtedly arises from phonon processes. Indeed, in our work to date we have been somewhat surprised that the lattice vibrations have not presented more of a problem. This phonon scattering is not observed at 80 °K simply because of the boson population factor which changes from 0.6 at 294 °K to 0.03 at 80 °K.

V. DISCUSSION AND CONCLUSIONS

From the analysis given in Sec. IV we see that the simple model of localized $4f$ electrons in an octahedral crystal field gives a good representation of the observed spectra for Tm^{3+} in TmSb. The relative intensities, line spacing, and temperature dependence of the spectra are well accounted for, and it is clear that the crystal-field eigenvalues and eigenfunctions for the energy levels are good approximations for this compound. The crystal-field parameters obtained at 80 °K are given in Eq. (7). These may be compared with the point-charge estimates of

$$A_4\langle r^4\rangle = 1.98Z \text{ meV} \ , \qquad A_6\langle r^6\rangle = 0.022Z \text{ meV} \tag{9}$$

calculated from Eq. (2) using $R = 3.042$ Å, $\langle r^4\rangle = 0.082$ Å^4, $\langle r^6\rangle = 0.078$ Å^6. The $\langle r^n\rangle$ were obtained by linear interpolation between the values given by Freeman and Watson[10] for Er^{3+} and Yb^{3+}. For the fourth-order term, therefore, we require $Z^{(4)} = 3.4$. This lies somewhat outside the range of values $2 < Z < 3$ which one might have expected using simple valency ideas, but it is not unreasonable. For the sixth-order term, however, one would require $Z^{(6)} \simeq 20$ which is clearly much too large. Inclusion of more-distant-neighbor effects does not alter these conclusions.[20] For the corresponding praseodymium compound PrSb, Turberfield *et al.*[9] find

$$A_4\langle r^4\rangle = 8.3 \pm 0.3(8.4) \text{ meV} \ , \qquad A_6\langle r^6\rangle = 0.17 \pm 0.07(0.14) \text{ meV} \ , \tag{10}$$

where the values in parentheses give the nearest-neighbor point-charge estimates using $Z = 2$. As noted previously, the choice $Z = 2$ also gives

quantitatively correct values for the other Pr^{3+} monopnictides and monochalcogenides.

We see, therefore, that the simple point-charge model which was surprisingly successful for the Pr^{3+} compounds is at best qualitatively correct for TmSb. It gives the proper order of magnitude for the dominant fourth-order term. However, it underestimates the sixth-order term by about a factor of 10. This large enhancement of the sixth-order term observed experimentally is, in fact, quite reminiscent of the situation commonly encountered in insulators.[20,21] Recent theory has ascribed this extra contribution to $A_6\langle r^6\rangle$ in insulators to overlap and covalency.[22,23] It is, however, somewhat puzzling that this enhancement effect seems to be significantly more important for Tm^{3+} compared with Pr^{3+}, whereas the $4f$ electrons in the former ion are much more compact than those in the latter ion.[10] Finally, the fact that $A_4\langle r^4\rangle$ exceeds the point-charge value indicates once more that the conduction electrons are not as effective in shielding the fourth-order crystal field as one might have thought at first.

It is of interest to reconsider Cooper and Vogt's measurements in light of our spectroscopic results. First, we do indeed confirm their conjecture that TmSb may be considered an ideal rare-earth intermetallic compound exhibiting crystal-field effects alone with negligible exchange. Furthermore, the explicit LLW crystal-field parameters we find fall within the range of values which they deduced. On the other hand, it is clear that only direct spectroscopic measurements can yield parameters of sufficient accuracy to be of any use in evaluating models for the microscopic origins of crystal fields in metals. It would be quite useful at this stage to repeat Cooper and Vogt's calculations of the single-crystal high-field magnetization using our more accurate crystal-field parameters. It seems likely from their paper that discrepancies of the order of 5–10% will still persist. These discrepancies could, of course, be experimental, nevertheless it seems possible that they may indicate the limiting accuracy of the model of localized $4f$ electrons in a static crystal field. Indeed, such discrepancies have already been found in insulators due to covalency[22,24] and virtual-phonon effects.[25]

Finally, these results illustrate the usefulness of inelastic neutron scattering for the study of Stark splittings in metals even in situations where the rare-earth ion has an angular momentum as large as $J=6$. A systematic study of crystal fields across an entire series of rare-earth metallic compounds would be most useful at this stage. We hope, also, that this work will serve to stimulate both fundamental theoretical research on the problem of crystal fields in metals and additional experimental work at other laboratories with neutron-scattering facilities.

ACKNOWLEDGMENTS

We would like to thank B. R. Cooper for a number of helpful discussions on his work with Vogt and on the subject of rare-earth intermetallic compounds in general. One of us (K. C. T.) would like to thank Brookhaven National Laboratory for their hospitality during the period that these measurements were carried out.

---

*Guest scientist at Brookhaven National Laboratory, Upton, N. Y.

†Work performed under the auspices of the U. S. Atomic Energy Commission.

[1]For a review, see S. Methfessel and D. C. Mattis, in *Handbuch der Physik*, edited by S. Flügge (Springer, New York, 1968), Vol. XVIII/1, p. 359.

[2]P. Junod, A. Menth, and O. Vogt, Physik Kondensierten Materie 8, 323 (1969).

[3]B. T. Matthias, R. M. Bozorth, and J. H. Van Vleck, Phys. Rev. Letters 7, 160 (1961).

[4]A. Jayaraman, V. Narayanamurti, E. Bucher, and R. G. Maines, Phys. Rev. Letters 25, 1430 (1970).

[5]B. R. Cooper and O. Vogt, Phys. Rev. B 1, 1218 (1970).

[6]K. Andres and E. Bucher, Phys. Rev. Letters 22, 600 (1969).

[7]R. J. Birgeneau, E. Bucher, L. Passell, D. L. Price, and K. C. Turberfield, J. Appl. Phys. 41, 900 (1970).

[8]K. C. Turberfield, L. Passell, R. J. Birgeneau, and E. Bucher, Phys. Rev. Letters 25, 752 (1970).

[9]K. C. Turberfield, L. Passell, R. J. Birgeneau, and E. Bucher, J. Appl. Phys. 42, 1746 (1971).

[10]A. J. Freeman and R. E. Watson, Phys. Rev. 127, 2058 (1962).

[11]B. R. Cooper and O. Vogt, Phys. Rev. B 1, 1211 (1970).

[12]See G. H. Dieke, *Spectra and Energy Levels of Rare Earth Ions in Crystals* (Wiley, New York, 1968).

[13]See, for example, M. T. Hutchings, Solid State Phys. 16, 227 (1964).

[14]K. W. H. Stevens, Proc. Phys. Soc. (London) A65, 209 (1952).

[15]K. R. Lea, M. J. M. Leask, and W. P. Wolf, J. Phys. Chem. Solids 23, 1381 (1962).

[16]P. de Gennes, in *Magnetism*, edited by G. T. Rado and H. Suhl (Academic, New York, 1963), Vol. 3, p. 115.

[17]R. J. Birgeneau, J. Phys. Chem. Solids (to be published).

[18]The sample was prepared in relatively conventional fashion. Thulium chips (spongelike material from distilled lumps) were reacted in antimony vapor in double sealed quartz tubes for about 49 h at 950 °C. The tubes had been previously sealed at ~5 μ of argon. The reaction product was then transferred under nitrogen gas in a tantalum crucible, pumped out, and subsequent-

ly sealed at 10^{-6} Torr. The material was then melted by resistance heating of the tantalum. The final sample was coarsely grained polycrystalline material with some single-crystal pieces as large as 0.1 cm^3. Resistivity measurements have been performed by Andres and Bucher (unpublished) on samples obtained from this batch and also on samples supplied by Vogt. They find that TmSb exhibits metallic behavior with a resistance ratio of about 18 and a residual resistivity of 1.4 $\mu\Omega$ cm at 1 °K.

[19]E. Bucher, K. Andres, J. P. Maita, A. S. Cooper, and L. D. Longinotti, J. Phys. (Paris) 32, 114 (1971).

[20]Only the second- and third-nearest neighbors are of any quantitative importance at all. They may be easily included in Eq. (2) by changing $Z(\mathrm{Sb})$ to

$$Z(\mathrm{Sb}) \rightarrow Z(\mathrm{Sb}) - [(2\sqrt{2}-1)/32]Z(\mathrm{Pr}) \text{ for } A_4\langle r^4\rangle,$$

$$Z(\mathrm{Sb}) \rightarrow Z(\mathrm{Sb}) - [(13\sqrt{2}-1)/128]Z(\mathrm{Pr}) \text{ for } A_6\langle r^6\rangle.$$

Since $Z(\mathrm{Pr}) \simeq -Z(\mathrm{Sb})$ this means that in the absence of shielding the second- and third-nearest neighbors increase the point-charge estimate of $A_4\langle r^4\rangle$ by $\sim 5.7\%$ and $A_6\langle r^6\rangle$ by $\sim 14\%$.

[22]J. D. Axe and G. Burns, Phys. Rev. 152, 331 (1966).

[23]R. E. Watson and A. J. Freeman, Phys. Rev. 156, 251 (1967).

[24]B. Bleaney, Proc. Roy. Soc. (London) A277, 289 (1964).

[25]R. J. Birgeneau, Phys. Rev. Letters 19, 160 (1967).

PHYSICAL REVIEW B VOLUME 4, NUMBER 3 1 AUGUST 1971

Nuclear Relaxation via a Two-Phonon Process in a Paramagnetic System*

B. Gregory and G. Seidel
Department of Physics, Brown University, Providence, Rhode Island 02912
(Received 5 March 1971)

The magnetic relaxation of the Co^{59} nucleus within the Co^{2+} ion in paramagnetic $Co(NH_4)_2(SO_4)_2 \cdot 6H_2O$ has been studied experimentally under the condition of nearly complete electron-spin alignment achieved at low temperatures (1 °K) and high magnetic fields (60 kG). An exponential variation of the nuclear relaxation time with temperature is found and ascribed to a two-phonon (Orbach) relaxation process operating through the intermediary of the upper levels of the electron-spin Kramers doublet. Calculations, in the spin-Hamiltonian framework, of the dependence of the relaxation time upon both temperature and magnetic field are presented which show this model to be in good agreement with experimental results. The relaxation time is of the form $T_1^{-1} = AH^7 e^{-g\mu_B H/kT}$. A theoretical relationship between the Orbach NMR relaxation time and the direct process ESR relaxation time is derived and compared with the available data.

I. INTRODUCTION

The nuclear magnetic resonance of Co^{59} in cobalt ammonium sulfate, $Co(NH_4)_2(SO_4)_2 \cdot 6H_2O$, has been discussed in some detail by Choh and Seidel.[1] They showed that it is possible to observe the NMR of the Co^{59} nucleus within the magnetic Co^{2+} ion by performing the resonance measurements at low temperatures and high magnetic fields such that the electronic moments are almost completely aligned by the Zeeman interaction with the external field. The purpose of that study was primarily to investigate the magnetic interaction between the nuclear moment and the electronic orbital moment induced by the external field.

In the course of pursuing the earlier measurements it was noted that the saturation characteristics of the NMR absorption lines were extremely sensitive to temperature. It is the purpose of this paper to describe the experimental results of a study of the relaxation behavior of the Co^{59} nucleus within the Co^{2+} ion and to present a theoretical explanation for the observed behavior.

II. SPIN HAMILTONIAN

The magnetic properties of the Co^{2+} ion in cobalt ammonium sulfate have been extensively studied by electron-spin resonance[2] as well as by NMR. The electronic ground-state Kramers doublet including interaction with the Co^{59} nucleus ($I = \frac{7}{2}$) can be described by the spin Hamiltonian as

$$\mathcal{H} = \mu_B \vec{H} \cdot \overleftrightarrow{g} \cdot \vec{S} + \vec{I} \cdot \overleftrightarrow{A} \cdot \vec{S} - \gamma\mu_N \vec{H} \cdot (\overleftrightarrow{1} + \overleftrightarrow{\sigma}) \cdot \vec{I} + \mathcal{H}_Q , \tag{1}$$

where the terms, written in order of descending magnitude, are the electronic Zeeman, hyperfine, nuclear Zeeman, induced-moment-nuclear, and quadrupole interactions. For tetragonal symmetry with the magnetic field at an angle θ with respect to the tetragonal axis, the Hamiltonian becomes